Molecular polarizability of water from local dielectric response theory

Xiaochuan Ge* and Deyu Lu†

Center for Functional Nanomaterials, Brookhaven National Laboratory, Upton, New York 11973, USA

(Received 2 June 2017; published 8 August 2017)

We propose a fully *ab initio* theory to compute the electron density response under the perturbation in the local field. This method is based on our recently developed local dielectric response theory [Phys. Rev. B **92**, 241107(R) (2015)], which provides a rigorous theoretical framework to treat local electronic excitations in both finite and extended systems beyond the commonly employed dipole approximation. We have applied this method to study the electronic part of the molecular polarizability of water in ice I*h* and liquid water. Our results reveal that the crystal field of the hydrogen-bond network has strong anisotropic effects, which significantly enhance the out-of-plane component and suppress the in-plane component perpendicular to the bisector direction. The contribution from the charge transfer is equally important, which increases the isotropic molecular polarizability by 5–6%. Our study provides insights into the dielectric properties of water, which form the basis to understand electronic excitations in water and to develop accurate polarizable force fields of water.

DOI: 10.1103/PhysRevB.96.075114

I. INTRODUCTION

Water is one of the most important substances for life, many fields of science, and numerous technological applications. Despite its simple molecular structure, water has many anomalous behaviors, e.g., its density reaching the maximum at 4 °C, that have attracted intensive research for decades. One intriguing aspect of the fundamental properties of water is the electronic excitation, which is essential to the understanding of a broad range of problems, such as solvation, water/solid interfaces, and electrochemical reactions in liquid solution. The quantum theory of electronic excitation has been widely used to interpret, e.g., the x-ray absorption [1–4] and optical absorption spectra of water [5,6], which in turn provide important physical insights into the atomic structures and the electronic structure of water. Besides, it has been well established that van der Waals dispersion forces, arising from the coupling of instantaneous and induced excitations, play a critical role in accurately describing the structure of water in *ab initio* molecular dynamics simulations [7–11].

In the linear response regime, how to describe the electronic part of the molecular polarizability of water (α_{H_2O}) remains a subject of debate, despite the rather simple textbook picture of dielectrics [12]. Experimentally, α_{H_2O} is known in the gas phase only [13]. In the condensed phase, the average value of the molecular polarizability is typically estimated from the refraction index measurement using the Lorentz-Lorenz relation [14]. Although this approach is suitable for gases and nonpolar liquids, it fails for polar liquids, such as water, due to the inaccurate description of the local field experienced by the polar molecule. Many competing models have been proposed to improve Debye's dipole theory [14], including models from Onsager [15] and Kirkwood [16]. Due to the deficiency of a classical treatment of the local field in liquid water, this problem has not been solved yet. Besides the actual value of α_{H_2O}, it is more important to understand how α_{H_2O} changes in different chemical environments (e.g., from the gas phase to the condensed phase) or under different boundary conditions (e.g., bulk water or confined water, such as water at the solid/water interface).

From the computational point of view, although the macroscopic average of the dielectric response of water is very well captured by the density functional theory (DFT) or beyond-DFT methods, such as the many-body perturbation theory [5,6], the chemical nature of the microscopic counterpart, e.g., the microscopic electric susceptibility (χ), remains poorly understood. Currently, a rigorous, fully *ab initio* theory to compute α_{H_2O} is lacking, and existing models predict contradicting trends in α_{H_2O}. Using point charge models to represent the solvent molecules, Gubskaya and Kusalik [17] found an increase of α_{H_2O} in liquid. Morita [18] proposed a cluster model, where the solute polarizability in the cluster is approximated by the difference of the polarizability of the cluster and that of the solvent only, $\Delta\alpha = \alpha^{\mathrm{tot}} - \alpha^{\mathrm{solv}}$. The nonadditive correction was taken into account by introducing a dielectric continuum model of the solvation shell [18]. In contrast to the point charge model, the cluster model predicts the isotropic molecular polarizability, $\bar{\alpha}_{H_2O} = \frac{1}{3}\mathrm{Tr}\,(\alpha_{H_2O})$, in the liquid is reduced from that in the gas phase by 7–9%, and the reduction was attributed to the electron repulsion of the ambient solvent molecules that perturb and confine the spatially diffuse tail of the electron cloud of the solute [18].

Most of other computational studies employed an extension [19] of the interactive dipole model (IDM) [20–22] to the condensed phase, where the electrostatics of the electron density response is approximated at the dipole-dipole interaction level. IDM calculations found that $\bar{\alpha}_{H_2O}$ in the liquid water is reduced by less than 2% [23,24] or the same as [25] that of the gas phase. These results also showed an anisotropic effect, with the in-plane components reduced, while the out-of-plane component enhanced [23–25]. The origin of these changes is unclear, as the effects of the crystal field are intertwined with structural changes of water monomer geometries under the thermal fluctuation.

Because of the uncertainties in determining α_{H_2O} from both experiment and theory, there is no clear recipe on how to choose the *right* α_{H_2O} in a polarizable force field, given the knowledge of the gas phase value [26]. To address this

*Present address: BlackRock, Inc.
†Email address: dlu@bnl.gov

open question, in this paper we proposed a fully *ab initio* method to compute α_{H_2O} based on our recently developed local dielectric response theory (LDRT) [27], which is among the techniques to compute the dielectric response function without explicitly referring to the empty states [28–34]. The new method is general and can be used to study α_{H_2O} in different chemical environments. We proved that the widely used IDM is the dipole limit of our theory. In the numerical study of α_{H_2O} in liquid water, we paid special attention to separate the environmental effects due to the crystal field and charge transfer from those caused by intramolecular thermal fluctuations.

II. METHOD

A. Molecular polarizability in extended systems under the dipole approximation

In order to quantify molecular polarizabilities in an extended system, it is necessary to express the dielectric response of a many-electron system in a local representation, instead of the Bloch representation. A formal way to proceed is to use the Wannier function (WF) formalism, such as the maximally localized Wannier function (MLWF) [35–37], where the WFs ($|w_{\mathbf{R}n}\rangle$) are constructed from unitary transformations of the Bloch orbitals ($|\psi_m^{\mathbf{k}}\rangle$). In systems with a finite band gap, we consider only the occupied bands:

$$|w_{\mathbf{R}n}\rangle = \frac{\Omega}{(2\pi)^3}\int_{BZ} d\mathbf{k} e^{-i\mathbf{k}\cdot\mathbf{R}} \sum_{m=1}^{n_v} U_{mn}^{(\mathbf{k})} |\psi_m^{\mathbf{k}}\rangle, \tag{1}$$

where n_v is the total number of the occupied bands, and Ω is the real space primitive cell volume. Unitary matrices ($U^{(\mathbf{k})}$) in the MLWF formalism minimize the spatial spreads of the WFs labeled by the lattice vector ($\mathbf{R}$) and the Wannier center index (n). In this study, we focus on isolated systems or periodic systems with a large supercell, where a single Γ-point sampling in the reciprocal space is used. The extension to general cases of the k-point sampling, although in principle feasible, is beyond the scope of this paper. In the Γ-point formulation, the above expression is simplified to

$$|w_n\rangle = \sum_{m=1}^{n_v} U_{mn}|\psi_m\rangle. \tag{2}$$

Within the modern theory of the electric polarization in crystalline dielectrics [38–41], the dipole moment of a subsystem (e.g., an ion or molecule labeled by M) is defined in atomic units as

$$\boldsymbol{\mu}_M = \sum_{i\in M} Z_i \boldsymbol{R}_i^{\text{ion}} - 2\sum_{n\in M} \boldsymbol{r}_n, \tag{3}$$

where Z_i and $\boldsymbol{R}_i^{\text{ion}}$ are the charges and positions of ions. Positions of the Wannier centers that belong to M, $\boldsymbol{r}_n = x_n\hat{i} + y_n\hat{i} + z_n\hat{k}$ can be computed from [35]

$$x_n = -\frac{L}{2\pi}\Im \ln\langle w_n|e^{-i\frac{2\pi}{L}x}|w_n\rangle, \tag{4}$$

where L is the size of the supercell.

Upon a small perturbation from an external electric field ($\boldsymbol{E}$) at a given frequency, the electronic contribution to the net induced dipole of M in the gas phase is given by

$$\Delta\boldsymbol{\mu}_M = \alpha_M^{\text{gas}}\ \boldsymbol{E}, \tag{5}$$

where α_M^{gas} is the frequency-dependent gas phase molecular polarizability tensor. Here we dropped the explicit frequency dependence to simplify the notation. Once the molecule is embedded in a chemical environment, e.g., a cation in a solid or a solute molecule surrounded by solvent molecules, the induced dipole arises from the response to the local field that is the sum of the external field and the induced field from the environment, $\boldsymbol{E}_M^{\text{loc}} = \boldsymbol{E} + \boldsymbol{E}_M^{\text{ind}}$. Unlike $\boldsymbol{E}$, $\boldsymbol{E}_M^{\text{ind}}$ is a microscopic quantity, whose direction and amplitude vary within the size of the molecule. In practice, this finite size effect is often ignored, which leads to the approximate expression,

$$\Delta\boldsymbol{\mu}_M = \alpha_M\ \boldsymbol{E}_M^{\text{loc}}, \tag{6}$$

where α_M is the environment-dependent molecular polarizability tensor.

Under the dipole approximation, $\boldsymbol{E}_M^{\text{ind}}$ in the IDM is approximated by the dipole field of environment molecules ($N \neq M$),

$$\boldsymbol{E}_M^{\text{ind}} \approx \sum_{N\neq M} T_{MN}\ \Delta\boldsymbol{\mu}_N, \tag{7}$$

where $T_{MN} = \nabla\nabla r_{MN}^{-1}$ is the dipole-dipole interaction tensor with r_{MN} the intermolecular distances. Substituting Eq. (7) into Eq. (6), one can derive an equation of interacting dipoles [19–22],

$$\Delta\boldsymbol{\mu}_M = \alpha_M\left(\boldsymbol{E} + \sum_{N\neq M} T_{MN}\ \Delta\boldsymbol{\mu}_N\right). \tag{8}$$

α_M in Eq. (8) can be solved conveniently, once $\Delta\boldsymbol{\mu}$ are obtained from finite external field calculations [19,24] or linear response theory [25].

B. Local dielectric response theory

Although the IDM combined with DFT has been widely used to calculate molecular polarizabilities [19,23–25,42], it has several drawbacks. First of all, as mentioned above, Eq. (6) neglects the finite size effect in the induced field of the environment. Secondly, the dipole approximation neglects all the higher order terms. It might be justifiable at the far field, but when molecules get close to each other, the validity of the dipole approximation is questionable. More severely, the use of T_{MN} does not satisfy the positive definite requirement of Eq. (8) [22]. As a consequence, molecular polarizabilities from the IDM can diverge or become negative in simple systems, e.g., the cooperative (head to tail) induced dipoles in the direction of the line connecting the two [22,43,44]. Finally, at the interface between M and the environment [see Fig. 1(b)], wave functions of excited environmental electrons can have finite overlap with the occupied valence electron orbitals of M, leading to a charge transfer (CT) type of density response on M. The CT contribution is a quantum effect and cannot be captured at the level of dipole-dipole interaction.

In order to develop a rigorous, fully quantum mechanical treatment of α_M, let us first consider a slightly broader scenario: The local excitations of a molecule embedded a

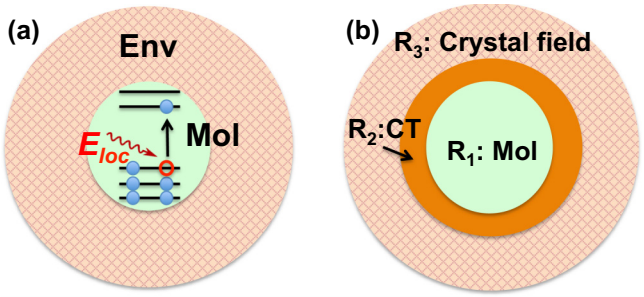

FIG. 1. (a) Schematics of local excitations of a molecule inside a chemical environment. (b) Three regions in the quantum mechanical description of the problem, $R_1 \in R_2 \in R_3$. R_1: the region of the molecule of interest, R_3: the whole system providing the crystal field (CF), and R_2: a subset of R_3 coupled to R_1 through charge transfer (CT) upon local excitations.

chemical environment as shown in Fig. 1(a). The whole system can thus be divided into three regions ($R_1 \in R_2 \in R_3$) as shown in Fig. 1(b), R_1: the region of the molecule of interest (M), R_3: the whole system providing the crystal field (CF), and R_2: a subset of R_3 coupled to R_1, such that CT can happen between R_2 and R_1 upon local excitations. We will introduce a formal theory based on the microscopic susceptibility χ. We note that Allen [44] developed a model of charge-dipole interaction along the same line, where charges are treated by quantum mechanics, and charge interactions are solved in the random phase approximation (RPA). The remaining obstacle in our approach is to reformulate χ, a nonlocal quantity by definition, in the local representation.

An early proposal was made by Hanke to address this issue by localizing electrons and holes separately when building an explicit electron-hole pair basis [45]. In practice, this method is inconvenient, because of (a) the difficulty to numerically converge the number of unoccupied bands and (b) even if the convergence can be reached, the poor locality of the high energy unoccupied bands. Both limitations of Hanke's method [45] can be avoided, because it is unnecessary to localize the unoccupied bands. In other words, we formulate the theory on the occupied manifold only, without using the explicit electron-hole pair basis. In the following, we first summarize the recently developed local dielectric response theory (LDRT) [27] that provides the theoretical framework to study local excitations. Then we use the LDRT to develop a fully *ab initio* theory to calculate the dielectric response of the perturbation in the local field.

The central quantities in the linear response theory are the bare, $\chi^0(\omega;\boldsymbol{r},\boldsymbol{r}')$, and the screened susceptibility, $\chi(\omega;\boldsymbol{r},\boldsymbol{r}')$, which are the functional derivatives of the charge density response with respect to perturbations in the self-consistent field potential ($\delta V_{\rm scf}$) and the external potential ($\delta V_{\rm ext}$):

$$\chi^0(\omega;\boldsymbol{r},\boldsymbol{r}') = \delta\rho(\omega;\boldsymbol{r})/\delta V_{\rm scf}(\omega;\boldsymbol{r}'),$$
$$\chi(\omega;\boldsymbol{r},\boldsymbol{r}') = \delta\rho(\omega;\boldsymbol{r})/\delta V_{\rm ext}(\omega;\boldsymbol{r}'). \quad (9)$$

In the following, we adopt the shorthand notation: $\Delta\rho = \chi^0\,\Delta V_{\rm scf} = \chi\,\Delta V_{\rm ext}$, where integration on common variables is implied. χ can be solved from χ^0 through Dyson's equation [46], $\chi = \chi^0 + \chi^0\,K\,\chi$, where $K = v_H + K_{xc}$ with v_H and K_{xc} being the Coulomb and exchange-correlation kernel, respectively. In the language of the linear response theory, χ^0 is the building block.

Under the Bloch representation, both $\Delta\rho$ and χ^0 can be partitioned according to occupied bands,

$$\Delta\rho = \sum_v \Delta\rho_v, \quad \chi^0 = \sum_v \chi^0_v,$$
$$\Delta\rho_v = \chi^0_v\,\Delta V_{\rm scf} = 2\,(|\Delta\psi^+_v\rangle + |\Delta\psi^-_v\rangle)\langle\psi_v|, \quad (10)$$

where $|\Delta\psi^\pm_v\rangle$ are the solution of the Sternheimer equation at $+$ and $-$ frequencies [29],

$$(\varepsilon_v - \hat{H} - \alpha\hat{P} \pm \omega)|\Delta\psi^\pm_v\rangle = \hat{Q}\,\Delta V_{\rm scf}|\psi_v\rangle. \quad (11)$$

Here ε_v are energy levels of the occupied states of the Kohn-Sham (KS) Hamiltonian ($\hat{H}$); $\hat{P} = \sum_v |\psi_v\rangle\langle\psi_v|$ and $\hat{Q} = \hat{I} - \hat{P}$ are projectors onto the occupied and unoccupied state manifolds, which are introduced to avoid the explicit reference to the unoccupied states [29]. The term $\alpha\hat{P}$ is introduced to remove the singularity of Eq. (11).

The essence of the LDRT is to recognize that $\Delta\rho$ is invariant under the unitary transformation of the occupied orbitals, which allows $\Delta\rho$ and χ^0 to be formulated under the Wannier representation,

$$\Delta\rho = \sum_n 2\,(|\Delta W^+_n\rangle + |\Delta W^-_n\rangle)\langle W_n|, \quad (12)$$

where $|\Delta W^\pm_n\rangle$ are solutions of the generalized Sternheimer equation [27],

$$\sum_{n'}(\tilde{\varepsilon}_{nn'} - \hat{H} - \alpha\hat{P} \pm \omega)|\Delta W^\pm_{n'}\rangle = \hat{Q}\Delta V_{\rm scf}|W_n\rangle. \quad (13)$$

Since $|W_n\rangle$ are not the eigenstates of the KS Hamiltonian, ε_v are replaced by the coupling matrix elements, $\tilde{\varepsilon}_{n,n'} = \langle W_n|H|W_{n'}\rangle$. In contrast to Eq. (11), linear response equations in Eq. (13) are entangled due to $\tilde{\varepsilon}_{n,n'}$. The variation of $|W_n\rangle$ caused by the perturbation at $|W_{n'}\rangle$ can be obtained from

$$|\Delta W^\pm_n\rangle = \sum_{n'} |\Delta W^\pm_{nn'}\rangle$$
$$\equiv \sum_{n'}[\tilde{\varepsilon} - (\hat{H} + \alpha\hat{P} \mp \omega)\,\hat{I}]^{-1}_{nn'}\,\hat{Q}\,\Delta V_{\rm scf}|W_{n'}\rangle, \quad (14)$$

where $\hat{I}$ is an $N_v \times N_v$ identity matrix. The indices of $\Delta W_{nn'}$ denote the perturbation site (right) and the response site (left), respectively. For systems with a finite band gap, Ge and Lu [27] proved that the spatial distribution of $|\Delta W^\pm_{nn'}\rangle$ decays exponentially in real space, and its magnitude decays exponentially as the distance between sites n and n'.

Combining Eqs. (13) and (14), one can formally construct the partial response densities and partial microscopic susceptibilities (PMSs) on Wannier centers according to

$$\Delta\rho = \sum_{nn'} \Delta\rho_{nn'}, \quad \chi^0 = \sum_{nn'} \chi^0_{nn'},$$
$$\Delta\rho_{nn'} = \chi^0_{nn'}\,\Delta V_{\rm scf} = 2\,(|\Delta W^+_{nn'}\rangle + |\Delta W^-_{nn'}\rangle)\langle W_n|. \quad (15)$$

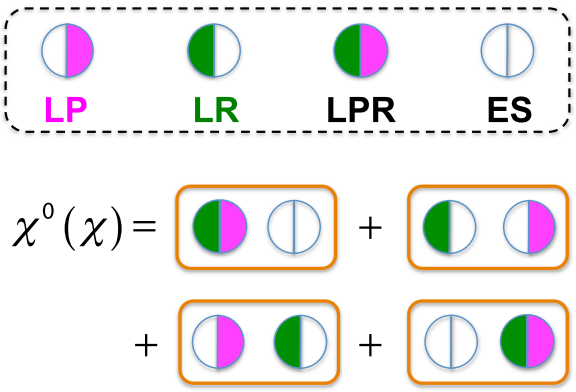

FIG. 2. Schematics of partitioning χ^0 (χ) of a system with two occupied Wannier orbitals into four partial microscopic susceptibilities. Diagrams at the top indicate all four possible scenarios on one site: local perturbation (LP), local response (LR), local perturbation plus local response (LPR), and an empty site (ES).

Similarly, χ can also be partitioned into PMSs through the Dyson's equation,

$$\chi_{nn'} = \sum_{n''} \sum_{m=0}^{\infty} \chi^0_{nn''} (K\,\chi^0)^m_{n''n'}. \tag{16}$$

The partition of χ^0 (χ) into PMSs is illustrated in Fig. 2 for a system with two occupied Wannier centers. On each site, there are four possible diagrams: local perturbation (LP) only, local response (LR) only, local perturbation plus local response (LPR), and an empty site (ES). Therefore, χ^0 (χ) of the whole system can be partitioned into four terms: two diagonal terms (LPR on site 1 and 2) and two off-diagonal terms (LP on one site and LR on the other site).

PMSs like $\chi_{nn'}$ are important quantities to study the nonlocality of the response functions. In particular, $\chi_{nn'}$ associates the response density at site n to the external perturbation, $\Delta V_{\rm ext}$, at site n'. In the quantum chemistry language, similar notions have been introduced based on the local basis set formalism in the conceptual density functional theory [47], to define the local reactivity index [48], the atom-condensed linear response matrix [49], and a measure of aromaticity [50,51]. It is worth noting that PMSs defined through the LDRT are formally additive and do not suffer basis set-dependent errors in the local basis set approach. By summing over the perturbation index, one can construct local response density, $\Delta\rho_n = \sum_{n'} \Delta\rho_{nn'}$, and local susceptibilities, $\chi^0_n = \sum_{n'} \chi^0_{nn'}$ and $\chi_n = \sum_{n'} \chi_{nn'}$, or their symmetric form, $\tilde{\chi}^0_n = \frac{1}{2}\sum_{n'}(\chi^0_{nn'} + \chi^0_{n'n})$ and $\tilde{\chi}_n = \frac{1}{2}\sum_{n'}(\chi_{nn'} + \chi_{n'n})$. A Dyson-like relation exists between χ_n and χ^0_n,

$$\chi_n = \chi^0_n (1 - K\chi^0)^{-1}. \tag{17}$$

χ_n provides a local measure of excited state properties projected onto a Wannier orbital, such as the bond polarizability [27].

C. Electronic density response of the local perturbation

We start by dividing the Wannier centers of the whole system into two subsystems: the molecule of interest (M) and the environment (E) as shown in Fig. 1(b). It is convenient to define local quantities associated with each subsystem, S ($S = M$ or E): $\Delta\rho_S = \sum_{n\in S} \Delta\rho_n$, $\chi^0_S = \sum_{n\in S} \chi^0_n$, and $\chi_S = \sum_{n\in S} \chi_n$. A quantum mechanical description of the molecular polarizability embedded in a medium relies on the density response to the perturbation in the local field, or in short, the local perturbation. Conceptually, within the linear response theory it implies (a) to freeze both the external perturbation potential and the induced potential due to the polarization of the environment and (b) to obtain the self-consistent solution of the response density of the molecule. In the same spirit, Buin and Iftimie [24] proposed the frozen orbitals polarizability model within the IDM based on the MLWFs, as an alternative to Heaton *et al.*'s formulation [19]. In practice, one has to "unscreen" (US) the PMSs on the molecule (χ_S) to remove the screening effects from the environment. For this purpose, we define the unscreened molecular susceptibility (χ^{us}_M) as

$$\Delta\rho_M = \chi^{us}_M\, \Delta V_{\rm loc}, \tag{18}$$

where $\Delta V_{\rm loc} = \Delta V_{\rm ext} + K\,\Delta\rho_M$ is the perturbation in the local potential. Clearly, this quantity is different from χ that is related to external perturbation, $\Delta V_{\rm ext}$, and χ^0 that is related to the self-consistent field perturbation, $\Delta V_{\rm scf}$. The unscreening procedure implies that

$$\chi^{us}_M = \chi^0_M + \chi^0_M\, K\, \chi^0_M + \chi^0_M \big(K\,\chi^0_M\big)^2 + \cdots = \chi^0_M + \chi^0_M\, K\, \chi^{us}_M. \tag{19}$$

The molecular polarizability is given by

$$\alpha_{M,ij} = -\int dr_i dr'_j\, r_i\, \chi^{us}_M(\omega;\boldsymbol{r},\boldsymbol{r}')\, r'_j \equiv -Tr\big[r_i\big(\chi^{us}_M r'_j\big)\big], \tag{20}$$

where i and j denote Cartesian axes. Because χ^0_M and χ_M are additive, so is the effective molecular polarizability, $\alpha^{\rm eff}_{M,ij} = -Tr[r_i(\chi_M r'_j)]$. On the other hand, because χ^{us}_M is not additive, neither is α_M.

In order to reveal the relation between the above quantum mechanical description and the IDM of Eq. (8), we similarly define χ^{us}_E as the unscreened susceptibility of the subsystem E under the perturbation of the local field,

$$\Delta\rho_E = \chi^{us}_E\, \Delta V_{\rm loc}. \tag{21}$$

It allows us to express the unscreened and screened susceptibilities of each subsystem,

$$\begin{aligned} \chi^{us}_S &= \chi^0_S (1 - K\chi^0_S)^{-1}, \\ \chi_S &= \chi^0_S (1 - K\chi^0)^{-1}. \end{aligned} \tag{22}$$

Employing the additivity relation, $\chi^0 = \chi^0_M + \chi^0_E$, we have

$$\chi_M = \chi^{us}_M + \chi^{us}_M\, K\chi_E, \tag{23}$$

$$\chi_E = \chi^{us}_E + \chi^{us}_E\, K\chi_M. \tag{24}$$

Consider $\Delta V_{\rm ext}(\boldsymbol{r}) = E_j\, r_j$. Multiply $-r_i$ from left and $E_j r'_j$ from right on both sides of Eq. (23) and integrate. It follows that

$$\Delta\mu_{M,i} = \alpha_{M,ij}\, E_j - Tr\big[r_i\big(\chi^{us}_M\, K\chi_E\, r'_j\big)\big]E_j. \tag{25}$$

Ignore K_{xc} in K and take the dipole approximation to expand $v_H = \sum_{N\in E} |(\boldsymbol{r}_M + \boldsymbol{r}'') - (\boldsymbol{r}_N + \boldsymbol{r}''')|^{-1}$ to the second order of r_{MN}. The only nonvanishing terms arise from $\boldsymbol{r}''\, T_{MN}\, \boldsymbol{r}'''$ due to the charge neutrality condition, $\int d\boldsymbol{r}\, \Delta\rho(\boldsymbol{r}) = 0$. Consequently, the second term on the right hand side of Eq. (25) becomes $\sum_{N\in E} \sum_{kl} \langle r_i|\chi_M^{us}|r_k''\rangle\, T_{MN,kl}\, \langle r_l'''|\chi_E|r_j'\rangle\, E_j$, where $T_{MN,kl} = \partial_k \partial_l r_{MN}^{-1}$. It is straightforward to show that

$$\Delta\mu_{M,i} = \alpha_{M,ij}\, E_j + \sum_{N\in E} \sum_{kl} \alpha_{M,ik}\, T_{MN,kl}\, \Delta\mu_{N,l}, \qquad (26)$$

which reproduces Eq. (8). Alternatively, by dividing E_j on both sides of Eq. (26), one obtains the IDM without explicit dependence on the external field,

$$\alpha_M^{\text{eff}} = \alpha_M + \sum_{N\in E} \alpha_M\, T_{MN}\, \alpha_N^{\text{eff}}. \qquad (27)$$

We have proved that the IDM is the classical limit of Eq. (23) under the dipole approximation.

One may also arrange the screened and unscreened PMSs in the matrix form through

$$\begin{pmatrix} \chi_M \\ \chi_E \end{pmatrix} = \begin{pmatrix} 1 & -\chi_M^{us}\, K \\ -\chi_M^{us}\, K & 1 \end{pmatrix}^{-1} \begin{pmatrix} \chi_M^{us} \\ \chi_E^{us} \end{pmatrix}. \qquad (28)$$

By expanding the matrix inversion in Taylor series, the first and second order corrections to χ_M are $\chi_M^{us}\, K\, \chi_E^{us}$ and $\chi_M^{us}\, K\, \chi_E^{us}\, K\, \chi_M^{us}$, respectively. In the limit that M and E are spatially fully separated, Dobson [52] derived the same low order correction terms to χ_M, which have been used by one of us to derive three-body terms in the RPA correlation energy [53]. Because Eq. (28) includes contributions at infinite orders, it is also valid in the regime where the electron densities of M and E overlap. We also note the similarity between Eq. (23) in this paper and Eq. (41) in the linear response theory of subsystem TDDFT [54,55].

III. COMPUTATIONAL DETAILS

In this study, ground state and linear response calculations were performed using the Perdew-Burke-Ernzerhof (PBE) [56] exchange-correlation functional with the SG15 optimized norm-conserving Vanderbilt (ONCV) pseudopotentials [57–59] together with the Γ-point sampling. The kinetic energy cutoff of the plane-wave basis set was chosen at 65 Rydberg. All the gas phase calculations were performed using a simple cubic supercell of 20 Å. MLWFs were constructed with Wannier90 [60]. α_M is calculated from the self-consistent solution of χ_M^{us} according to Eq. (19) through the DFPT implemented in a customized version of QUANTUM ESPRESSO [61]. At each self-consistent step, the generalized Sternheimer equations are solved, and the density response is projected onto M as $\Delta\rho_M = \chi_M^0\, \Delta V_{\text{loc}}$. The converged density response is used to compute α_M.

In practice, we first compute the ground state of the system, which can be either a finite system in a supercell or an extended system described under the periodic boundary condition. Since we are using a Γ-point formalism for extended systems, the unit cell size has to be sufficiently large. Next we construct Wannier orbitals for occupied states, and associate Wannier orbitals to their corresponding water molecules. Different environmental effects can be quantified separately based on the choices of R_1, R_2, and R_3 denoted by $(n_{R_1} : n_{R_2} : n_{R_3})$ in the subsequent linear response calculations. Each of R_1, R_2, and R_3 denotes a subset of water molecules. Specifically in the study of α_{H_2O}, R_1 is restricted to one water molecule, i.e., $n_{R_1} = 1$. For the CF effect, R_3 contains the whole system, which means that V_{scf} of the whole system is used in the Sternheimer equations. We restrict the charge transfer effects inside the subsystem defined by R_2. If $n_{R_2} = n_{R_3}$, no truncation is applied, and the generalized Sternheimer equations are solved for all the occupied Wannier orbitals. If $n_{R_2} < n_{R_3}$, the generalized Sternheimer equations are truncated so that only the occupied Wannier orbitals corresponding to R_2 are included.

The effect of the crystal field is investigated by comparing water clusters with different sizes with extended systems. To this end, we consider two extended systems (ice I*h* and liquid water) and three types of water clusters: water monomers ($n_{R_3} = 1$), water clusters including the first solvation shell ($n_{R_3} = 5$), and water clusters including the first and second solvation shells ($n_{R_3} = 17$). The structures of gas phase water clusters are fixed at the same geometry as those in ice I*h* or liquid water in order to eliminate the ambiguity due to the structural changes. To study the distance dependence of the CT effect, the region of R_2 is varied in size, with the lower limit being one water molecule (R_1) and the upper limit being the whole system (R_3).

The ice I*h* structure is modeled by an orthorhombic supercell ($n_{R_3} = 96$; $a = 13.30$ Å, $b = 15.36$ Å, and $c = 14.47$ Å) constructed from the hexagonal unit cell ($a = b = 7.78$ Å, $c = 7.33$ Å, and $\gamma = 60°$) of Ref. [62]. Although the effect of proton disorder can in principle be studied by using different proton-ordered, energetically quasidegenerate ice I*h* structures, it is beyond the scope of the current paper. The structures of liquid water were taken from the trajectories of the *ab initio* molecular dynamics simulation of 64-molecule water samples at 400 K, the water PBE400 dataset [63] ($n_{R_3} = 64$). The supercell size is 12.41 Å. α_{H_2O} are averaged over the first 20 snapshots of the PBE400_64 subset, resulting in 1280 water molecule geometries.

IV. RESULTS AND DISCUSSIONS

A. Water monomer in the gas phase

α_{H_2O} of the gas phase water monomer optimized with the PBE exchange-correlation functional is listed in Table I. $\bar{\alpha}_{H_2O} = 1.59$ Å^3, and the three principal components are $\alpha_{xx} = 1.58$ Å^3, $\alpha_{yy} = 1.60$ Å^3, and $\alpha_{zz} = 1.58$ Å^3, respectively. The principal axes are defined as the following: x along the bisector direction, y along the in-plane perpendicular direction, and z along the normal direction of the molecular plane. These values are in close agreement with the previous PBE results [25]. $\bar{\alpha}_{H_2O}$ overestimates the experimental value by 8%, in line with the error expected from PBE. This overestimation is associated with the underestimation of band gap and band width well known for semilocal approximations to the exchange and correlation potential and in line with Penn's model [64] of the dielectric constant. Nevertheless, our main focus is to understand the general trend of the environmental effects on

TABLE I. Molecular polarizability of water (in Å^3) of the gas phase monomer, ice I*h*, and liquid water. Results in liquid water are the statistical average ($\langle\alpha\rangle$) and the standard deviation (σ). The x axis is the dipole axis, and the z axis is the normal direction of the molecular plane. Gas phase molecules in the rows of ice I*h* and liquid water have the same geometry as in the condensed phase. CF and CT denote the crystal field and charge transfer, respectively.

		α_{xx}	σ_{xx}	α_{yy}	σ_{yy}	α_{zz}	σ_{zz}	$\bar{\alpha}_{H_2O}$	σ
monomer	PBE[a]	1.58		1.60		1.58		1.59	
	BLYP[b]	1.60		1.63		1.59		1.61	
	BLYP[b,c]	1.47		1.53		1.42			
	exp[d]	1.468 ± 0.003		1.528 ± 0.013		1.415 ± 0.013		1.470 ± 0.003	
ice I*h*	gas phase	1.65		1.71		1.61		1.66	
	CF	1.58		1.44		1.76		1.60	
	CF + CT	1.69		1.54		1.88		1.70	
water	gas phase	1.64	0.05	1.69	0.08	1.61	0.03	1.65	0.05
	CF	1.66	0.10	1.55	0.09	1.78	0.14	1.66	0.08
	CF + CT	1.76	0.11	1.63	0.10	1.86	0.16	1.75	0.09
	BLYP[b]	1.45		1.42		1.48			
	BLYP[c]	1.44	0.03	1.41	0.03	1.49	0.03		

[a]This work.
[b]Reference [23].
[c]Reference [24].
[d]Reference [13].

α_{H_2O} in the condensed phase, i.e., changes in α_{H_2O}, not the absolute value.

We also checked our gas phase results using the BLYP functional [65,66] in order to compare with the BLYP results in the literature [23,24]. As shown in Table I, BLYP results in Refs. [23,24] are systematically smaller than our results, with $\bar{\alpha}_{H_2O}$ about 8% smaller than our result. This difference is caused by the supercell size convergence issue in the finite field calculations [67] in previous studies [23,24]. As pointed out by Buin and Iftimie [24], α_{xx} obtained from a 10 Å cubic box is known to underestimate the fully converged value by 8%, and similar underestimations are likely to occur also in their liquid water calculations. Their observation is consistent with the fact that α_{xx} in Refs. [23,24] is about 8% smaller than our result. On the other hand, our linear response method does not suffer this convergence issue. For example, gas phase α_{ii} calculated with 20 Å and 30 Å cubic supercells are within 0.04%. If we compare PBE and BLYP results in this paper, $\bar{\alpha}^{BLYP}_{H_2O}$ is slightly larger than $\bar{\alpha}^{PBE}_{H_2O}$ by 1%.

B. Isotropic molecular polarizability of water

Environmental effects on $\bar{\alpha}_{H_2O}$ in ice I*h* are shown in Fig. 3. Because the geometries of each water molecule in the ground state ice I*h* model are almost identical, the computed $\bar{\alpha}_{H_2O}$ differ by less than 0.15%. Therefore we present the results from a single water molecule in ice I*h*. We consider four systems: three gas phase water clusters with $n_{R_3} = 1$ (monomer), 5 (first shell), and 17 (second shell) and ice I*h* with $n_{R_3} = 96$. Here gas phase clusters refer to water molecules with the same geometry as in ice I*h* to enable a straight comparison. First, we focus on the CF effect by fixing $n_{R_2} = 1$ and varying $n = n_{R_3}$. The effect of the CF is to reduce $\bar{\alpha}_{H_2O}$. Compared to $\bar{\alpha}_{H_2O} = 1.66$ Å^3 of the gas phase monomer, $\bar{\alpha}_{H_2O}$ decreases by 3.1% caused by the CF of the first solvation shell. When the full CF of ice I*h* is included, $\bar{\alpha}_{H_2O}$ decreases by 3.8%. Gubskaya and Kusalik [17] reported an opposite trend, i.e., an increase of $\bar{\alpha}_{H_2O}$ by $1.2 \sim 5.3\%$, which is likely due to the approximate nature of their local field models represented by the electrostatic field of a few point charges.

Next, we analyze the CT effect in ice I*h* by fixing $n_{R_3} = 96$ and varying $n = n_{R_2}$. In general, we expect the CT effect to enhance α_M, as the excitation of neighboring water molecules

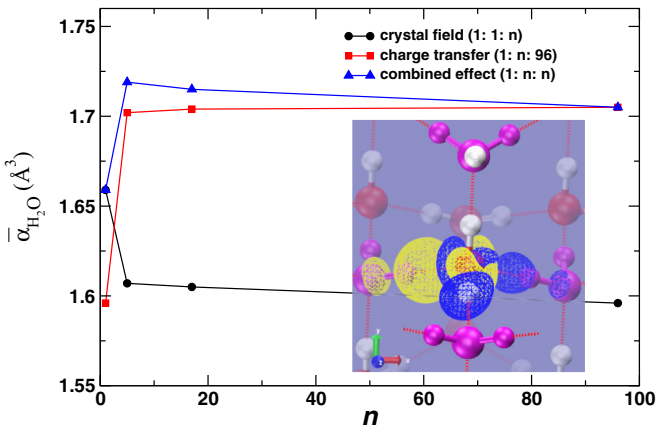

FIG. 3. Environmental effects on the isotropic molecular polarizability of water ($\bar{\alpha}_{H_2O}$) in ice I*h*. Notation ($n_{R_1} : n_{R_2} : n_{R_3}$) corresponds to the number of water molecules in the molecular region (n_{R_1}), the charge transfer region (n_{R_2}), and the crystal field region (n_{R_3}) as defined in Fig. 1 and Sec. III. Inset shows the isosurface of the electron density response due to the charge transfer under a uniform electric field along the x axis (the red arrow), i.e., $\Delta\Delta\rho^{CT} = \Delta\rho(1,96,96) - \Delta\rho(1,1,96)$. Yellow indicates electron accumulation; blue indicates electron depletion. Water molecules are visualized in the ball-and-stick representation with oxygen and hydrogen atoms represented by red and white spheres. The four water molecules tetrahedrally H-bonded to the central water molecule are highlighted in purple. The isosurface plot was generated with VMD [68].

has a constructive contribution. Indeed after we include the CT effect from the first solvation shell, $\bar{\alpha}_{H_2O}$ increases from 1.60 to 1.70 Å^3, which is more significant than the total CF effect. Since the CT effect is short ranged, it saturates readily at $n_{R_2} = 5$. At $n_{R_2} = 96$, $\bar{\alpha}_{H_2O}$ further increases by only 0.003 Å^3. Finally, we combine the CF and CT effects by simultaneously varying $n = n_{R_2} = n_{R_3}$. As shown in Fig. 3, the CT effect dominates within the first solvation shell, and $\bar{\alpha}_{H_2O}$ reaches the maximum at 1.72 Å^3. Beyond that, the CT effect fades away, and the tail of the CF effect takes over. $\bar{\alpha}_{H_2O}$ decreases slowly by 0.01 Å^3 at $n = 96$. Overall, $\bar{\alpha}_{H_2O}$ in ice I*h* is larger than the gas phase value by 2.8%.

The inset of Fig. 3 shows the isosurface of the electron density response in ice I*h* due to the charge transfer under a uniform electric field along the x axis (the red arrow), i.e., $\Delta\Delta\rho^{CT} = \Delta\rho(1,96,96) - \Delta\rho(1,1,96)$. Clearly one can see a positive induced dipole moment emerging from the four nearest neighbor water molecules (highlighted in purple) that are H-bonded to the central water molecule. Previously, Lu *et al.* [69] applied the MLWF procedure to localize the eigenvectors of the static dielectric matrices in ice I*h* and liquid water and identified dominant screening modes that are either localized on individual water molecules or involving H-bonded water dimers. Based on our study, the physical origin of these modes becomes clear, which are intramolecular excitations and intermolecular charge transfer excitations.

Next we compute $\bar{\alpha}_{H_2O}$ in liquid water, where the thermal disorder effects play a key role in contrast to the results of ice I*h* at zero temperature. Here we divided the thermal disorder effects into intramolecular contributions on individual water molecules and intermolecular contributions from the crystal field including H-bonds and long-range electrostatic effects. To isolate the intramolecular component, we sampled $\bar{\alpha}_{H_2O}$ of gas phase water monomers with the same geometries as those in liquid water. The intermolecular contributions were extracted by comparing $\bar{\alpha}_{H_2O}$ of the gas phase and liquid water that includes environmental effects.

As shown in Table I and Fig. 4, $\langle\bar{\alpha}_{H_2O}\rangle$ is 1.65 Å^3 in the gas phase, which is averaged over 1280 monomer configurations. Here $\langle\cdots\rangle$ denotes the statistical average. This mean value is nearly the same as that in ice I*h* (1.66 Å^3), and the intramolecular thermal disorder in the PBE water leads to a standard deviation of $\sigma = 0.05$ Å^3. However, once the CF effect is included, $\langle\bar{\alpha}_{H_2O}\rangle$ slightly increases to 1.66 Å^3, which is substantially larger than that in ice I*h* (1.60 Å^3) by 4%. At the same time, σ increases to 0.08 Å^3, indicating a notable intermolecular contribution. The effect of the CT in liquid water is similar to that in ice I*h*, which further increases $\bar{\alpha}_{H_2O}$ by 0.09 Å^3 with σ almost unaffected. This suggests that the crystal field is the primary source of the intermolecular thermal disorder effects.

C. Anisotropic effects of the molecular polarizability of water

The crystal field in the condensed phases can modify the electronic properties of individual water molecules significantly. For example, solvated water molecules form hydrogen bonds (H bonds) with their neighbors in a tetrahedral geometry,

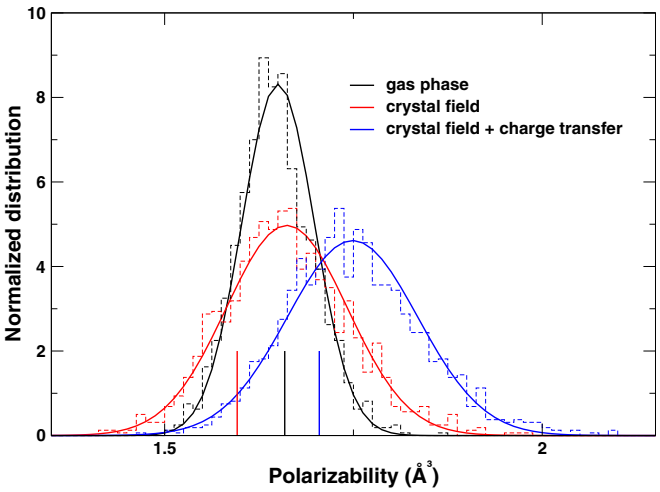

FIG. 4. Distributions of the isotropic molecular polarizability of water ($\bar{\alpha}_{H_2O}$) in liquid water. Short vertical lines indicate corresponding values in ice I*h*.

which has a strong influence on the Wannier function centers (WFCs: two from the O-H covalent bonds and two from the oxygen lone pairs). As a consequence, the O-H bond WFCs are pulled in and the lone pair WFCs are pulled out as compared to the gas phase monomer [70]. In order to gain insights into the chemical origin of the CF and CT effects, we examine the anisotropic effects in ice I*h* and liquid water by decomposing the α_{H_2O} tensor onto three internal principal axes and correlating the changes in the molecular polarizability ($\Delta\alpha_{ii}, i = x,y,z$) with the changes in the O-WFC pair correlation function, $g(r)$, in terms of $\Delta r_{\text{O-WFC}}$.

As shown in Table I, the CF of ice I*h* causes α_{xx} and α_{yy} to decrease by 4% and 16% and α_{zz} to increase by 9%. It appears that the in-plane suppression effect is more pronounced in the y direction. Interestingly, this anisotropic CF effect can be qualitatively captured using the point charge model [17] except for the x component, which yields $\Delta\alpha_{xx} = 4\%$, $\Delta\alpha_{yy} = -4\%$, and $\Delta\alpha_{zz} = 16\%$ from their model II. This strong anisotropic CF effect is thus characteristic of the H-bond network in the condensed phase. On the other hand, the effect of the CT is mostly isotropic, increasing each component by about 0.1 Å^3.

Similar to the isotropic molecular polarizability, $\langle\alpha_{ii}\rangle$ of gas phase monomers in liquid water (1.64, 1.69, and 1.61 Å^3) are very close to those in ice I*h* (1.65, 1.71, and 1.61 Å^3) as shown in Table I and Fig. 5, with the largest deviation of 1% from the y direction. The largest spread is also found in the y direction ($\sigma_{yy} = 0.08$ Å^3), followed by x ($\sigma_{xx} = 0.05$ Å^3) and z ($\sigma_{zz} = 0.03$ Å^3). The CF in liquid water also exhibits a significant anisotropic effect, which leads to $\Delta\langle\alpha_{ii}\rangle = +1\%$, -9%, and $+11\%$ as compared to the gas phase values. Another important feature is that the z component acquires the largest spread ($\sigma_{zz} = 0.14$ Å^3), and the spreads in x and y directions are much smaller ($\sigma_{xx} = 0.10$ Å^3 and $\sigma_{xx} = 0.09$ Å^3). The CT effect in liquid water increases $\langle\alpha_{ii}\rangle$ almost uniformly by 0.1 Å^3, and the spreads are only slightly increased.

The origin of the CF effects in ice I*h* and liquid water was investigated using $\Delta r_{\text{O-WFC}}$, which are the differences of O-WFC distances between the condensed phases and the

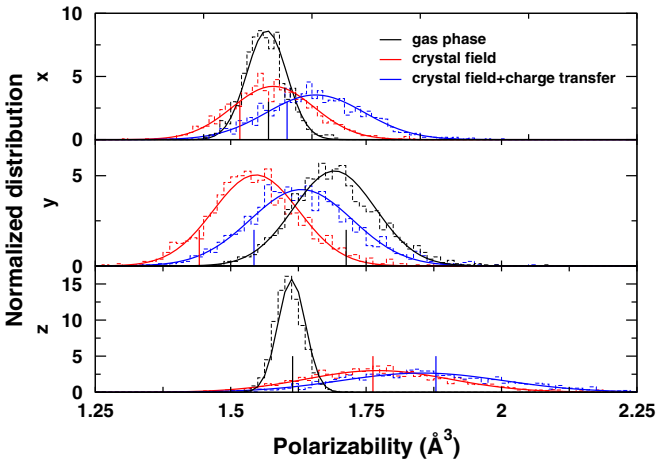

FIG. 5. Distributions of the molecular polarizability of water in liquid water along three principal directions (x: bisector direction, y: in-plane perpendicular direction, and z: out-of-plane direction). Short vertical lines indicate corresponding values in ice Ih.

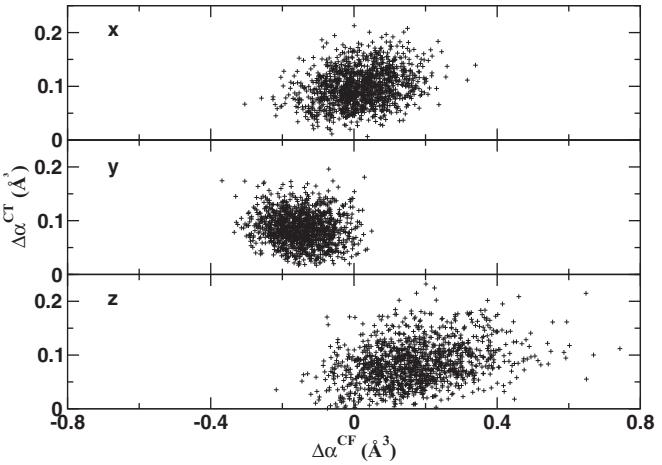

FIG. 7. Correlation between the crystal field (CF) and charge transfer (CT) contributions in the molecular polarizability of water in liquid water.

gas phase. As shown in Fig. 6, in ice Ih $\Delta r_{\text{O-WFC}} = 0.05$ and -0.04 Å for the oxygen lone pair and the O-H bond, respectively. In other words, O-H bond WFCs are pulled in from 0.53 Å by 0.04 Å, while lone pair Wannier centers are pulled out from 0.30 Å by 0.05 Å as compared to the gas phase monomer, in line with the established trend in liquid water [70]. The formation of the H bonds therefore weakens the intramolecular O-H bond, making it more ionic, and loosens the oxygen lone pairs. Since the O-H WFs become more tightly bound to the oxygen atom, the in-plane components of α_{H_2O} are suppressed. In contrast, since the lone pair WFs become more loosely bound to the oxygen atom, the out-of-plane component is enhanced. In liquid water, both changes get smaller, i.e., $\Delta\langle r_{\text{O-WFC}}\rangle = 0.03$ and -0.03 Å, indicating overall softer H bonds than ice Ih. Consequently, the CF effects have a smaller impact on the in-plane components of liquid water ($\Delta\langle\alpha_{xx}\rangle = 1\%$ and $\Delta\langle\alpha_{yy}\rangle = -9\%$) than ice

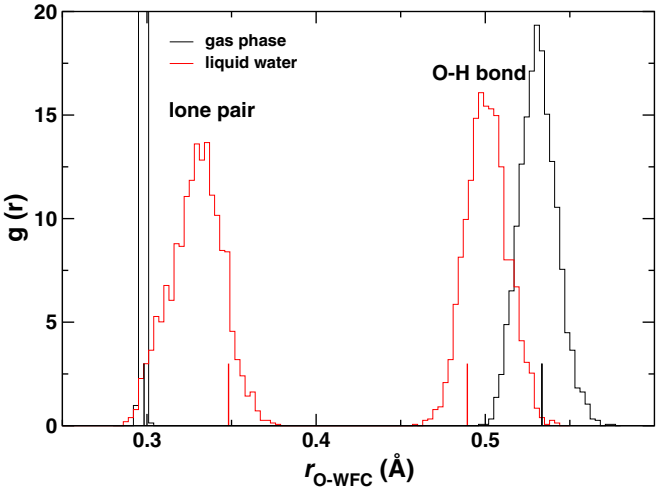

FIG. 6. Pair correlation function of the oxygen-Wannier function centers (O-WFCs) in liquid water. Short vertical lines indicate corresponding values in ice Ih.

Ih ($\Delta\alpha_{xx} = -4\%$ and $\Delta\alpha_{yy} = -16\%$), while $\Delta\langle\alpha_{zz}\rangle$ in both systems are comparable (11% and 9%). The oxygen lone pair has a larger spread ($\sigma_{\text{O-WFC}} = 0.015$ Å) than the O-H bond ($\sigma_{\text{O-WFC}} = 0.012$ Å), which is consistent with the largest spread in α_{zz} (see Fig. 5 and Table I).

To investigate any possible correlation between the CF and CT effects in liquid water, we track $\Delta\alpha_{ii}$ from CF and CT effects for each water molecule. As shown in Fig. 7, while the distribution of $\Delta\alpha_{xx}^{\text{CF}}$ is nearly symmetric around zero, the signs of $\Delta\alpha_{yy}^{\text{CF}}$ and $\Delta\alpha_{zz}^{\text{CF}}$ are opposite, with one being predominantly negative and the other positive. No apparent correlation was found for the in-plane components, while there is a weak correlation between $\Delta\alpha_{zz}^{\text{CF}}$ and $\Delta\alpha_{zz}^{\text{CT}}$. Therefore our procedure of treating CF and CT effects separately is justified.

The main differences between our model and previous models can be understood as the following. In the point charge model [17], the CF is over-simplified. In the IDM, although the full CF is included at the ground state level, the Coulomb kernel is approximated by the dipole interaction. It is not straightforward to compare the absolute values of α_{H_2O} of this work with the IDM results in the literature [23,24], because different exchange-correlation functionals (PBE and BLYP) were used, and results in previous studies are likely not fully converged. A likely meaningful comparison is the trend of the environmental effects on α_{H_2O} with respect to the gas phase values computed from the optimized geometry. In this paper, the relative changes of $\langle\alpha_{ii}\rangle$ are 11%, 6%, and 18% in x, y, and z, respectively. The trends are qualitatively different from the IDM that yields $-2 \sim -1\%$, $-8 \sim -7\%$, and $4 \sim 5\%$, respectively [23,24]. Besides the effects from different functionals, these differences may be attributed to several limitations in the IDM, such as the lack of the finite size effect and the use of the dipole-dipole approximation.

In summary, we have developed a fully *ab initio* method to compute the electron density response to the perturbation in the local field based on the local dielectric response theory. We applied this method to compute the molecular polarizability of water in condensed phases. Using the same molecular geometries as in the condensed phases, we found

that the effects of the crystal field is to reduce α_{yy} and enhance α_{zz} and that the charge transfer effect increases all the principal components uniformly. Our study provides a rigorous theoretical framework to determine α_{H_2O}, essential to both the physical understanding of water and computer simulations using polarizable force field models. As the electron-based spectroscopy techniques, e.g., electron energy loss spectroscopy (EELS), has reached subangstrom spatial resolution [71], we expect these experimental techniques can provide more details about the microscopic dielectric response of water in the future.

ACKNOWLEDGMENTS

We thank M. Hybertsen, X. Wu, R. Car, A. Selloni, P. B. Allen, and M. Pavanello for their helpful discussions. This research used resources of the Center for Functional Nanomaterials, which is a US DOE Office of Science Facility, at Brookhaven National Laboratory under Contract No. DE-SC0012704. This research used resources of the National Energy Research Scientific Computing Center, a DOE Office of Science User Facility supported by the Office of Science of the US Department of Energy under Contract No. DE-AC02-05CH11231.

[1] M. Cavalleri, H. Ogasawara, L. Pettersson, and A. Nilsson, Chem. Phys. Lett. **364**, 363 (2002).
[2] B. Hetényi, F. De Angelis, P. Giannozzi, and R. Car, J. Chem. Phys. **120**, 8632 (2004).
[3] D. Prendergast and G. Galli, Phys. Rev. Lett. **96**, 215502 (2006).
[4] W. Chen, X. Wu, and R. Car, Phys. Rev. Lett. **105**, 017802 (2010).
[5] P. H. Hahn, W. G. Schmidt, K. Seino, M. Preuss, F. Bechstedt, and J. Bernholc, Phys. Rev. Lett. **94**, 037404 (2005).
[6] V. Garbuio, M. Cascella, L. Reining, R. Del Sole, and O. Pulci, Phys. Rev. Lett. **97**, 137402 (2006).
[7] B. Santra, A. Michaelides, M. Fuchs, A. Tkatchenko, C. Filippi, and M. Scheffler, J. Chem. Phys. **129**, 194111 (2008).
[8] C. Zhang, J. Wu, G. Galli, and F. Gygi, J. Chem. Theory Comput. **7**, 3054 (2011).
[9] B. Santra, J. Klimeš, D. Alfè, A. Tkatchenko, B. Slater, A. Michaelides, R. Car, and M. Scheffler, Phys. Rev. Lett. **107**, 185701 (2011).
[10] J. Wang, G. Román-Pérez, J. M. Soler, E. Artacho, and M.-V. Fernández-Serra, J. Chem. Phys. **134**, 024516 (2011).
[11] M. J. Gillan, D. Alfè, and A. Michaelides, J. Chem. Phys. **144**, 130901 (2016).
[12] C. Kittel, *Introduction to Solid State*, Vol. 162 (John Wiley & Sons, New York, 1966).
[13] W. F. Murphy, J. Chem. Phys. **67**, 5877 (1977).
[14] P. Debye, Ann. Phys. **344**, 789 (1912).
[15] L. Onsager, J. Am. Chem. Soc. **58**, 1486 (1936).
[16] J. G. Kirkwood, J. Chem. Phys. **7**, 911 (1939).
[17] A. Gubskaya and P. Kusalik, Mol. Phys. **99**, 1107 (2001).
[18] A. Morita, J. Comput. Chem. **23**, 1466 (2002).
[19] R. J. Heaton, P. A. Madden, S. J. Clark, and S. Jahn, J. Chem. Phys. **125**, 144104 (2006).
[20] L. Silberstein, Philos. Mag. **33**, 92 (1917); **33**, 215 (1917); **33**, 521 (1917).
[21] J. Applequist, J. R. Carl, and K.-K. Fung, J. Am. Chem. Soc. **94**, 2952 (1972).
[22] B. T. Thole, Chem. Phys. **59**, 341 (1981).
[23] M. Salanne, R. Vuilleumier, P. A. Madden, C. Simon, P. Turq, and B. Guillot, J. Phys.: Condens. Matter **20**, 494207 (2008).
[24] A. Buin and R. Iftimie, J. Chem. Phys. **131**, 234507 (2009).
[25] Q. Wan, L. Spanu, G. A. Galli, and F. Gygi, J. Chem. Theory Comput. **9**, 4124 (2013).
[26] J. W. Ponder, C. Wu, P. Ren, V. S. Pande, J. D. Chodera, M. J. Schnieders, I. Haque, D. L. Mobley, D. S. Lambrecht, R. A. DiStasio Jr *et al.*, J. Phys. Chem. B **114**, 2549 (2010).
[27] X. Ge and D. Lu, Phys. Rev. B **92**, 241107(R) (2015).
[28] S. Baroni, P. Giannozzi, and A. Testa, Phys. Rev. Lett. **58**, 1861 (1987).
[29] S. Baroni, S. de Gironcoli, A. Dal Corso, and P. Giannozzi, Rev. Mod. Phys. **73**, 515 (2001).
[30] H. F. Wilson, F. Gygi, and G. Galli, Phys. Rev. B **78**, 113303 (2008).
[31] H. F. Wilson, D. Lu, F. Gygi, and G. Galli, Phys. Rev. B **79**, 245106 (2009).
[32] B. Walker, A. M. Saitta, R. Gebauer, and S. Baroni, Phys. Rev. Lett. **96**, 113001 (2006).
[33] D. Rocca, R. Gebauer, Y. Saad, and S. Baroni, J. Chem. Phys. **128**, 154105 (2008).
[34] D. Rocca, D. Lu, and G. Galli, J. Chem. Phys. **133**, 164109 (2010).
[35] N. Marzari and D. Vanderbilt, Phys. Rev. B **56**, 12847 (1997).
[36] I. Souza, N. Marzari, and D. Vanderbilt, Phys. Rev. B **65**, 035109 (2001).
[37] N. Marzari, A. A. Mostofi, J. R. Yates, I. Souza, and D. Vanderbilt, Rev. Mod. Phys. **84**, 1419 (2012).
[38] R. D. King-Smith and D. Vanderbilt, Phys. Rev. B **47**, 1651 (1993).
[39] D. Vanderbilt and R. D. King-Smith, Phys. Rev. B **48**, 4442 (1993).
[40] I. Souza, T. Wilkens, and R. M. Martin, Phys. Rev. B **62**, 1666 (2000).
[41] R. Resta, Rev. Mod. Phys. **66**, 899 (1994).
[42] B. Rotenberg, M. Salanne, C. Simon, and R. Vuilleumier, Phys. Rev. Lett. **104**, 138301 (2010).
[43] P. T. Van Duijnen and M. Swart, J. Phys. Chem. A **102**, 2399 (1998).
[44] P. B. Allen, J. Chem. Phys. **120**, 2951 (2004).
[45] W. R. Hanke, Phys. Rev. B **8**, 4585 (1973).
[46] A. L. Fetter and J. D. Walecka, *Quantum Theory of Many-Particle Systems* (Courier Corporation, New York, 2003).
[47] P. Geerlings, F. De Proft, and W. Langenaeker, Chem. Rev. **103**, 1793 (2003).
[48] M. Torrent-Sucarrat, P. Salvador, M. Solà, and P. Geerlings, J. Comput. Chem. **29**, 1064 (2008).

[49] N. Sablon, F. De Proft, and P. Geerlings, J. Phys. Chem. Lett. **1**, 1228 (2010).
[50] N. Sablon, F. De Proft, M. Solà, and P. Geerlings, Phys. Chem. Chem. Phys. **14**, 3960 (2012).
[51] S. Fias, P. Geerlings, P. Ayers, and F. De Proft, Phys. Chem. Chem. Phys. **15**, 2882 (2013).
[52] J. F. Dobson, in *Topics in Condensed Matter Physics*, edited by M. P. Das (Nova, New York, 1994), Chap. 7.
[53] D. Lu, H.-V. Nguyen, and G. Galli, J. Chem. Phys. **133**, 154110 (2010).
[54] M. Pavanello, J. Chem. Phys. **138**, 204118 (2013).
[55] A. Krishtal, D. Sinha, A. Genova, and M. Pavanello, J. Phys.: Condens. Matter **27**, 183202 (2015).
[56] J. P. Perdew, K. Burke, and M. Ernzerhof, Phys. Rev. Lett. **77**, 3865 (1996); **78**, 1396 (1997).
[57] D. R. Hamann, Phys. Rev. B **88**, 085117 (2013).
[58] M. Schlipf and F. Gygi, Comput. Phys. Commun. **196**, 36 (2015).
[59] http://www.quantum-simulation.org/potentials/sg15_oncv/
[60] A. A. Mostofi, J. R. Yates, G. Pizzi, Y.-S. Lee, I. Souza, D. Vanderbilt, and N. Marzari, Comput. Phys. Commun. **185**, 2309 (2014).
[61] P. Giannozzi, S. Baroni, N. Bonini, M. Calandra, R. Car, C. Cavazzoni, D. Ceresoli *et al.*, J. Phys.: Condens. Matter **21**, 395502 (2009).
[62] B. Santra, J. Klimeš, A. Tkatchenko, D. Alfè, B. Slater, A. Michaelides, R. Car, and M. Scheffler, J. Chem. Phys. **139**, 154702 (2013).
[63] http://www.quantum-simulation.org/reference/h2o/pbe400/s32/index.htm
[64] D. R. Penn, Phys. Rev. **128**, 2093 (1962).
[65] A. D. Becke, Phys. Rev. A **38**, 3098 (1988).
[66] C. Lee, W. Yang, and R. G. Parr, Phys. Rev. B **37**, 785 (1988).
[67] P. Umari and A. Pasquarello, Phys. Rev. B **68**, 085114 (2003).
[68] W. Humphrey, A. Dalke, and K. Schulten, J. Mol. Graphics **14**, 33 (1996).
[69] D. Lu, F. Gygi, and G. Galli, Phys. Rev. Lett. **100**, 147601 (2008).
[70] P. L. Silvestrelli and M. Parrinello, Phys. Rev. Lett. **82**, 3308 (1999).
[71] M. D. Kapetanakis, W. Zhou, M. P. Oxley, J. Lee, M. P. Prange, S. J. Pennycook, J. C. Idrobo, and S. T. Pantelides, Phys. Rev. B **92**, 125147 (2015).